Chapter 7
Structure and Function of Molecular Machines

7.1 Channels and Pores

We have seen in chapter 4 that passive diffusion of ions and small molecules across membranes occurs most efficiently when facilitated by pores, channels and carriers. Furthermore, in chapter 6 we discussed that certain gated structures had to exist for controlling the membrane permeability to ions during the generation and propagation of action potentials. These are now known as *ion channels*, and their presence and biological role has been convincingly revealed in electrophysiological studies even before high resolution structural studies became available. By contrast to channels and pores, ion pumps transport specific ions against concentration gradients across the membrane, and they do so by consuming energy produced in cellular processes.

The rate of channel-facilitated diffusion is 10^7–10^8 ions/s, more than 1,000 times higher than the rate of ion transport by ionic pumps. This rate is almost as high as that of free diffusion of ions in an aqueous solution. However, ion channels are not simple pipelines; instead, they possess a complex structure, which is sensitive to environmental changes. Channels present roughly two conformational states: *open* and *close*. Depending on the specific role of a channel and its location, transition between these two states (called *gating* or *activation*) may be triggered by various factors as summarized next.

(a) *Chemical activation* (ligand-gated) – by attachment of a specific ligand to the channel, as in the case of aquaporin (see below), G-protein-coupled channels (or receptors), and channels that detect the neurotransmitter acetylcholine
(b) *Electrical activation* (voltage-gated) – by a depolarizing electrical field, as for Na^+ and K^+ channels
(c) *Mechanical activation* (mechanically-gated) – by the action of an external force, torque, or pressure (e.g., channels in mechanosensory neurons)
(d) *Light-based activation* (light-gated) – induced by absorption of a photon, such as in the case of rhodopsin

We will discuss briefly the connection between structural and functional aspects of single channels in the next two sub-sections, while a summary of the current knowledge regarding the structure and function of ion pumps will be presented in section 7.1.2; particular emphasis will be put on *Na, K^+-ATPase*, which performs simultaneous countertransport of Na^+ and K^+ against their respective concentration gradients.

7.1.1 Electrical Behavior of Individual Ion Channels

Single ion channels had been investigated using electrical methods long before their structures were determined with high resolution. The main technique used in electrical studies of single channels – the *patch-clamp technique* – has evolved from the *voltage-clamp technique* (see chapter 6), primarily through refinements introduced in the micropipette method by Neher and Sakmann (Neher, 1991; Neher and Sakmann, 1976, 1992).

The patch clamp technique uses a voltage-clamp amplifier (similar to the one shown in Fig. 6.7) to fix the transmembrane voltage, and a glass pipette with a micrometer-sized tip for electrical current measurements. Alternatively, one may fix the current and measure the voltage. The smooth, round tip (diameter $\sim 1\,\mu m$) of the pipette is pressed against the cell membrane, while suction (i.e., "negative pressure") is applied to seal the contact with the cell. The interior of the pipette is filled with solutions containing electrolyte and other chemicals, to ensure electrical contact between the membrane patch and electronics, and provide means for controlling the behavior of the ion channels present in the patch of the membrane.

Reducing the *Johnson thermal noise* of the current source (i.e., the membrane patch) was the major hurdle that had to be overcome in the development of the patch-clamp technique (Neher, 1991). This noise is in addition to the noise introduced by the electronics and appears in the amplified signal in parallel to the signal from the membrane patch. To measure small currents generated at the passage of ions through single channels, large internal impedances of the source of current are necessary, which can be achieved with small signal sources: membrane patches. For that purpose, the contact between the microelectrode and the cell membrane has to be unusually good. The critical "ingredient" is the slight suction applied to the pipette to tightly seal the electrolyte in the interior of the pipette from the medium around the cell.

Quiz 1. The Johnson thermal noise can be expressed as the root-mean-square deviation (σ) of the current and depends on the absolute temperature (T), the measurement bandwidth (Δf) and the internal resistance of the signal source (R), as given by the following expression:

$$\sigma = \left(4k_B T \frac{\Delta f}{R}\right)^{1/2},$$

where k_B is Boltzmann's constant. Determine the internal resistance of the source necessary to measure a current of 1 pA at $\Delta f = 1\,\text{kHz}$ with 10% accuracy.

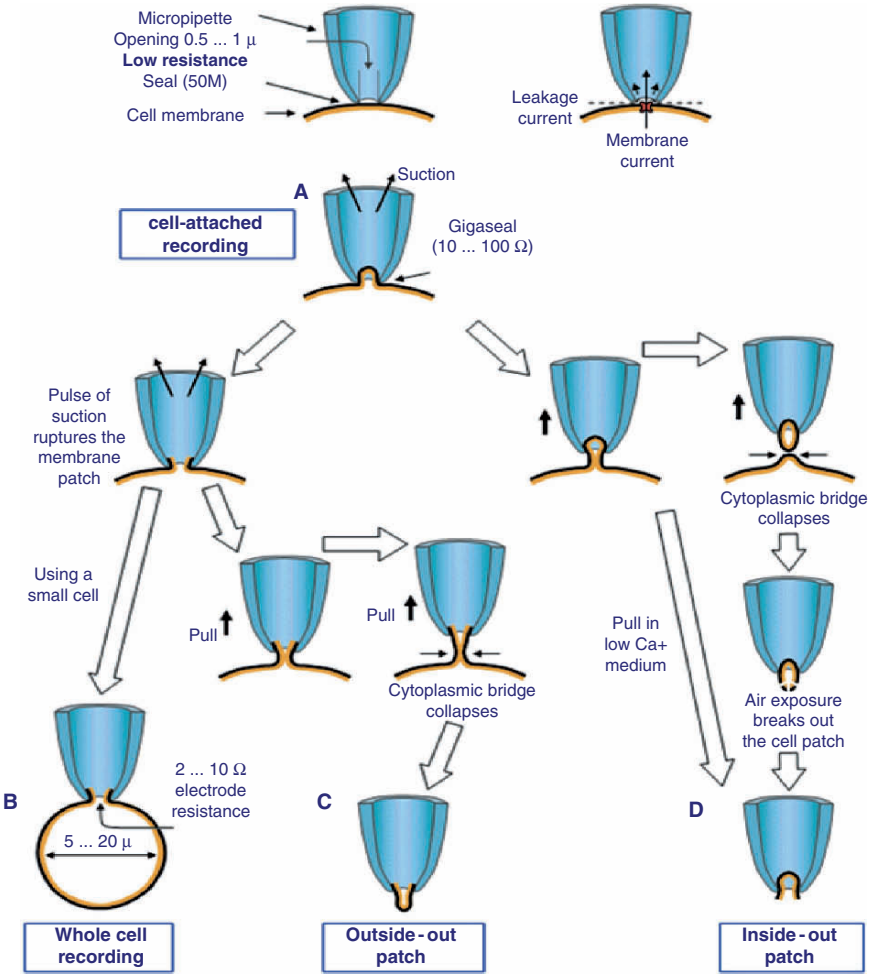

Fig. 7.1 Possible configurations of micropipette-membrane attachment (Reproduced from Neher and Sakmann, 1992).

Depending on the purpose of the measurements, various configurations of the cell-pipette contact are used, as shown in Fig. 7.1 and briefly described below.

Cell-attached recording (top of Fig. 7.1). By applying slight suction to the end of the pipette opposite to the tip, the seal between the tip and the membrane is improved to the extent that single-channel signals may be distinguished from background noise. This configuration is good for measurements on single channels that happen to be in the area of the patch.

Whole-cell recording. Applying a short pulse of suction may rupture the membrane patch, and an electrical contact may be established with the interior of the cell. The method measures all the ion channels in the membrane and is similar to

the microelectrode penetration technique illustrated in chapter 6 (Fig. 6.1), with the significant difference that it is less invasive to the cell (due to the smaller opening in the cell membrane). In addition, it opens a way for inserting various chemicals inside the cell, as necessary in experiments.

Inside-out patch. While in the whole-cell configuration (i.e., after the patch has been ruptured), the pipette may be pulled away from the membrane so that the cell and the patch separate from one another at their juncture and seal themselves from the external medium. The membrane patch trapped at the tip of the micropipette may be used to investigate the behavior of single channels under cytoplasmic fluid regulation.

Outside-out patch. Starting again from the cell-attached configuration, while the membrane is subjected to slight suction, and pulling the pipette away from the membrane, the patch detaches from the membrane and seals to form a small vesicle trapped at the tip of the micropipette. This configuration may be used to investigate the behavior of single channels activated by extracellular receptors.

In summary, three of the configurations described above could be used for detection of single channel currents under the effect of various endogenous or exogenous regulators. Figure 7.2 gives an example of single-channel signal obtained from patch-clamp measurements. The on-off behavior of the current suggests the channel transition between its "open" and "close" states.

The impact of the patch-clamp technique upon electrophysiological studies of ion channels has been tremendous, in particular by proving the existence of the gated structures hypothesized by Hodgkin and Huxley to explain the action potential. Detailed information on electrophysiological characterization of ionic channels is presented in a number of excellent books (see, e.g., Sakmann and Neher, 1995; Malmivuo and Plonsey, 1995; Hille, 2001). For their work on developing the patch-clamp technique on single ion channels behavior, Neher and Sakmann have been awarded the Nobel Prize in Physiology or Medicine in 1991 (Neher, 1991; Sakmann, 1991).

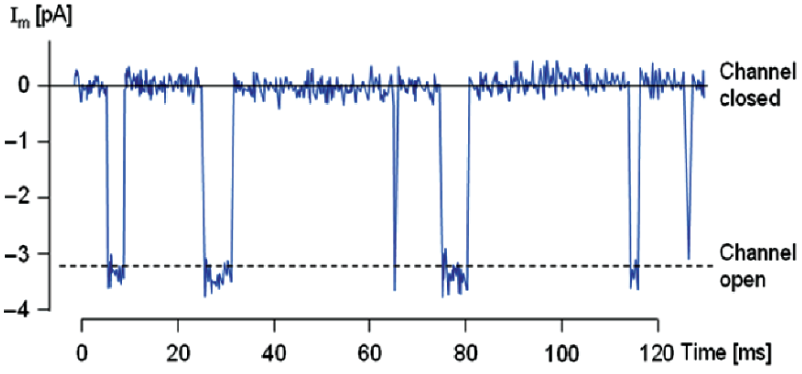

Fig. 7.2 Example of channels signal from patch-clamp measurements of a single ion channel at the neuromuscular endplate of frog muscle fiber (From Malviuo and Plonsey, 1995).

7.1.2 Structural Characterization by X-Ray Crystallography

In this section, we shall present the basic notions and concepts of X-ray crystallography (Rhodes, 1993; Drenth, 1994), with particular emphasis on the way in which they are applied to protein structure determinations.

The idea of using crystals to achieve X-ray diffraction has been credited to Max von Laue, who, together with two technicians, subjected a sphalerite [i.e., $(Zn, Fe^{2+})S$] crystal to X-rays and recorded a pattern of well-defined spots caused by diffraction. The method has evolved rapidly, notably through the work of the Braggs, father and son, who were able to determine the structure of many crystalline substances (and received the Nobel Prize in 1915). The first protein structure determination was reported by John Kendrew and co-workers (Kendrew et al., 1958) for myoglobin. For his work, Kendrew received Nobel Prize in Chemistry in 1962 (along with his colleague, Max Perutz).

A real breakthrough in the interpretation of X-ray diffraction on crystalline materials was conceiving the diffraction as a *selective reflection* of X-rays on the atoms pertaining to the *reticular planes* of the crystals (Fig. 7.3). According to this view, the constructive interference of the diffracted rays is obtained only if the *Bragg-Bragg formula* is obeyed:

$$2d_{hkl} \sin \alpha_n = n\lambda;\ n = 1, 2, \ldots \tag{7.1}$$

where λ is the wavelength of the selectively reflected X-rays and α_n are the incidence/reflection angles.

In order for X-ray diffraction to occur, the protein of interest needs to be crystallized, most often as a dimeric or larger unit (Drenth, 1994). The X-ray photons are scattered by the electronic clouds of the atoms comprising the macromolecules (Fig. 7.4). Since the macromolecules are located at regular positions within the crystal, the scattered photons interfere to form distinct patterns at the plane of detection.

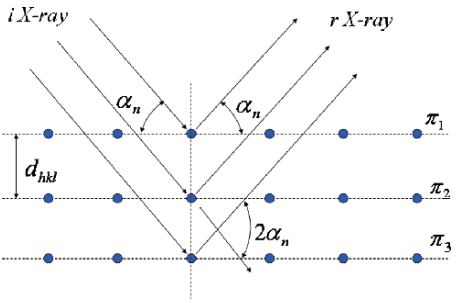

Fig. 7.3 X-ray selective reflection on the crystal atoms (filled circles) pertaining to the reticular plane family $\pi_i (i = 1, 2, \ldots)$ described by the Miller indices *hkl*. Notations: *i X-ray* – incident X-rays; *r X-ray* – reflected X-rays; d_{hkl} – distance between two adjacent reticular planes of the family (*hkl*).

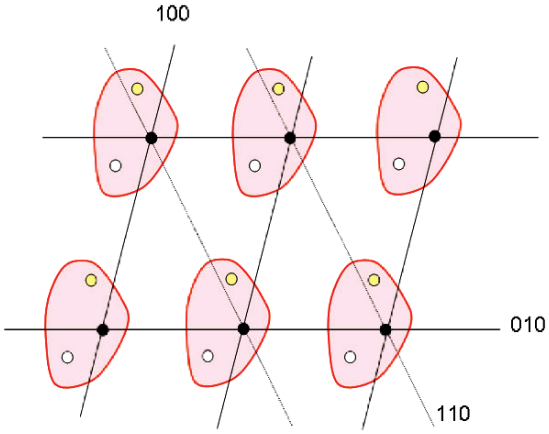

Fig. 7.4 Schematic representation of a small fraction of a protein crystal. The protein is shown as a large contour, in which three atoms are highlighted. As one can easily see, the atoms represented by same color (or same gray level) form a lattice in which they are lying on a family of atomicly smooth mirror planes indicated by their Miller index. The same argument holds for all atoms in the protein and also for the center of mass of each molecule (represented in black). This can be generalized: Each family of planes crossing the lattice points connect equivalent molecules and are, therefore, mirror planes.

X-ray scattering is stronger for atoms with larger atomic number, Z, due to the higher electron density of those atoms. In the case of proteins, however, the constitutive elements are usually elements with low atomic numbers, ^{1}H, ^{6}C, ^{8}O, and ^{16}S, and only rarely ^{26}Fe, ^{27}Co, and ^{30}Zn (which also appear in small quantities in prosthetic groups), so that the proteins diffract X-rays only slightly.

One can enrich proteins with heavy metal ions, and compare the diffraction patterns of the native protein with the one with heavy atoms added. Most protein crystals used in X-ray crystallography contain a known number of heavy metal ions (e.g., $^{78}Pt^{2+}$, $^{80}Hg^{2+}$) attached in known positions to the protein chain (such as, for instance, to the –SH groups of Cysteine). The process of inserting heavy ions into protein chains must conserve the crystal original form, with the exception that certain atoms are replaced; that means that the original and modified proteins are isomorphous. In practice, multiple isomorphic derivatives of a macromolecule need to be studied, in order to overcome the ambiguity related to an absence of the phase information (see below).

Because a crystal presents spatial periodicity, its centers of diffraction (i.e., the electronic clouds of its atoms) may be described as being situated in different reticular planes characterized by the *Miller indices* h, k, and l. As a result of scattering on regularly distributed centers, and of the interference (Fig. 7.3), a mathematical transformation is effectively performed of a 3-D structure (not yet known) into an experimentally measurable 2-D diffraction image. More precisely, diffraction performs a *Fourier transform* of a periodic arrangement in the real 3-D space (i.e., the 3-D structure) to render an image in the *inverse* Fourier space. Therefore, the problem of resolving the 3D structure is equivalent to performing an *inverse Fourier*

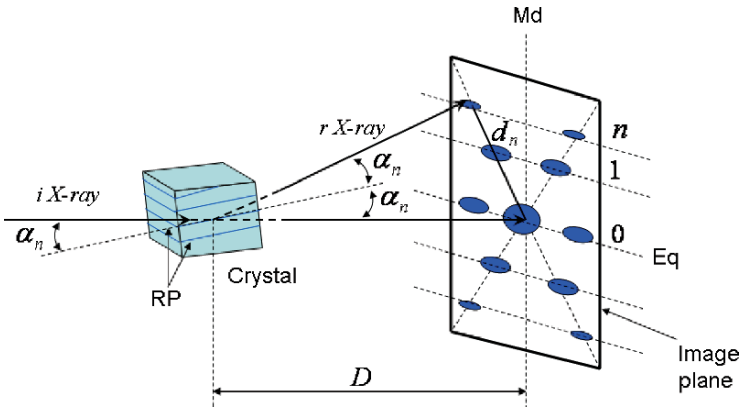

Fig. 7.5 Schematic depiction of the X-ray diffraction (or selective reflection) by a crystal and the diffraction image in the case of a fibrillar macromolecule. Notations: *i X-ray* – incident X-rays; *r X-ray* – reflected X-rays; RP – equivalent reticular planes inside the crystal; D – distance between crystal and image plane; Eq – equator of the image; Md – meridian of the image; n – order of diffraction; d_n – distance between the central diffraction spot (originating from the undiffracted X rays) and the nth order diffraction spot; α_n – incidence/reflection angle.

transform from the experimentally-recorded diffraction image back into the real 3-D space in which the unknown structure is embedded.

From Fig. 7.5, one may observe that the diffraction/reflection angle entering equation (7.1) obeys the relation:

$$\alpha_n = \frac{1}{2}\arctan(d_n/D) \tag{7.2}$$

A crystal structure may be obtained formally by repetitive arrangement of an elementary structure along three directions in space, *Ox, Oy* and *Oz* (which are not necessarily perpendicular to one another). This repetitive unit is called the *unit cell* of the crystal and is characterized by three sides $(\vec{a},\vec{b},\vec{c})$ and three angles (α,β,γ), as shown in Fig. 7.6.

The inverse Fourier transform of the diffraction image obtained from proteins described by, e.g., an orthorhombic system (with $a \neq b \neq c, \alpha = \beta = \gamma = 90^\circ$, see Fig. 7.6) gives the electron density as:

$$\rho(x,y,z) = \frac{1}{V}\sum_h\sum_k\sum_l F(hkl)e^{-2\pi i(hx/a+ky/b+lz/c)} \tag{7.3}$$

where V is the volume of the unit cell, $F(hkl)$ are structure factors associated with the reticular planes (hkl), and $i = (-1)^{1/2}$. The summation in (7.3) is made over all the reticular planes (in principle, h, k, and l vary from $-\infty$ to $+\infty$), each family of parallel reticular planes contributing to a diffraction peak in the diffraction image. The higher the order of diffraction spots that can be measured the better the resolution of the recovered electron density. Therefore, reticular planes with higher Miller indices are important only because they improve resolution.

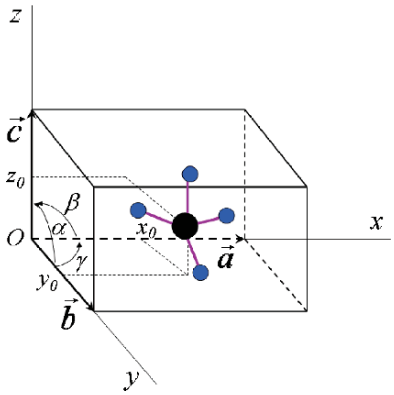

Fig. 7.6 Schematic representation of a unit cell associated with the crystal of a hypothetical molecule composed of five atoms, four of which are identical. The central atom (large filled circle) has the coordinates $x_0 = a/2,\ y_0 = b/2,\ z_0 = c/2$.

The structure factors, $F(hkl)$, are complex quantities which may be expressed as:

$$F(hkl) = |F(hkl)|\, e^{i\alpha(hkl)} \tag{7.4}$$

where $|F(hkl)|$ represent the magnitudes of *F(hkl)* and $\alpha(hkl)$ are their phase. The magnitudes may be directly related to experimentally measurable intensities, $I(hkl)$, of the diffraction spots, according to:

$$|F(hkl)| = \sqrt{I(hkl)/K} \tag{7.5}$$

where K is a known experimental factor. By contrast, the phases are much more difficult to recover experimentally, although they too are required for carrying out the triple summation in equation (7.3). Phase recovery constitutes one of the greatest challenges in 3D protein structure determination from X-ray diffraction. In practice, there are methods to recover the structure factor phases, which include *multiple isomorphous replacement* of certain atoms by heavy metal ions, all of which are quite laborious.

If the primary structure of the protein is known and once phases are determined, at least partially, determination of the spatial arrangements of atoms in the protein (i.e., the tertiary and quaternary structure) may proceed. First, the known magnitudes and the approximate phases of the structure factors are introduced into expression (7.3) to compute the approximate electron density. From this, one can deduce the approximate spatial coordinates $[(x_i,\ y_i,\ z_i),\ i = 1,\ 2, \ldots,\ \mathrm{N})]$ of the N atoms in the protein. At this point, one can obtain better approximations of the phases, $\alpha_1^c(hkl)$, from the approximate spatial coordinates and by using a direct Fourier transform. The new phases are re-introduced into expression (7.3) together with the experimentally determined magnitudes of the structure factors, from which improved estimates of the electronic densities, $\rho_1(x_i^1,\ y_i^1,\ z_i^1)$, are obtained, which

lead to a new set of phases, $\alpha_2^c(hkl)$, and so on. The process of structure refinement continues until a so-called *reliability factor*,

$$R_i = \frac{\left| \sum_h \sum_k \sum_l |F^{ex}(hkl)| - |F_i^c(hkl)| \right|}{\sum_h \sum_k \sum_l |F^{ex}(hkl)|} \tag{7.6}$$

which is determined at each refinement step, i, from computed (superscript "c"), and measured (superscript "ex") $|F(hkl)|$ values, decreases below an arbitrarily set value of 0.25; this value is usually regarded as a good practical limit. The structure of the macromolecule thus obtained may be represented graphically, by using computer programs, in various ways – as, protein backbone, ribbon representation, etc. – as shown in section 2.2.1.4.

Maintaining the X-ray diffraction's dominant role in structural molecular studies has been made possible by steady increase in sensitivity of diffractometric techniques and by notable advances in obtaining high quality protein crystals. However, exhausting the pool of crystallizable proteins is a growing challenge in X-ray crystallography which needs to be overcome if it were to at least maintain, if not to increase, the current pace of protein structure determinations. In chapter 2, we have mentioned a possible way for circumventing this problem.

7.2 X-Ray Investigations of Channels and Pores

Much of the knowledge of channels structure and function accumulated over the past few decades originated from electrophysiological and other biophysical studies – including patch-clamp – which were often coupled with artificially induced genetic mutations in the channels that affected their function. X-ray diffraction studies of channels and pores have been hampered by difficulties in obtaining crystals of such proteins, which, as discussed in section 2.2, constitutes the major problem with X-rays studies of most membrane proteins. This situation has persisted until relatively recently, when the success of Roderick MacKinnon and his colleagues in crystallizing channel proteins has led to a series of breakthroughs in the study of high-resolution channel structures (Doyle et al., 1998; Dutzler et al., 2002; Jiang et al., 2003).

As shown in Fig. 7.7, several classes of channels form *oligomeric complexes* of identical monomeric units. While voltage-dependent potassium channels and ligand-gated cation or anion channels form a single pore at the center of the oligomeric structure, the monomers of the voltage-gated chlorine channels and the ligand-gated aquaporin possess their own individual pores (Jensch, 2002). In this chapter, we discuss the general structural and functional features of the potassium and chlorine channels. For ligand-gated channels, such as the *aquaporin*, the reader is referred to the literature in the field (see, e.g.: Törnroth-Horsefield et al., 2006).

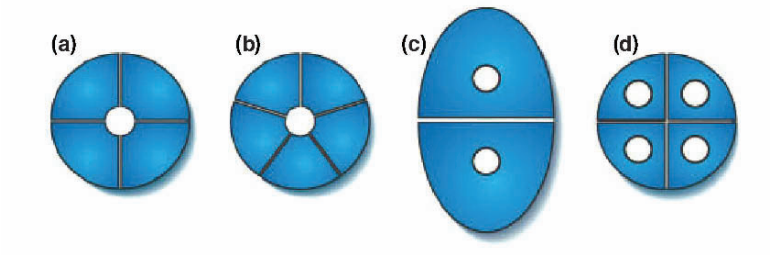

Fig. 7.7 Schematic representation of different types of oligomeric assemblies of protein subunits, or monomers: (**a**) tetrameric potassium channels and (**b**) ligand-gated ion channels (such as the gamma-aminobutyric acid-gated, or GABA-gated channels) forming a single central pore; (**c**) chlorine channels; and (**d**) water channels (aquaporin) forming two or more pores (Figure from Jentsch, 2002).

Figure 7.8 shows the tetrameric structure as seen from two perpendicular directions of a voltage-gated K^+ channel determined from X-ray crystallography (Doyle et al., 1998). The transmembrane helices form a hydrophilic pore, padded generously with water molecules, for the passage if ions through the otherwise hydrophobic core of the membrane.

The permeability of the channel is controlled by a fast and highly efficient voltage-sensitive gate that switches the channel between an *open* and a closed *state*. From studies of several K^+ channels, a common feature has emerged that the voltage sensor, formed by charged helices whose charges, may move across the membrane following changes in the transmembrane potential (Jiang et al., 2003). This motion probably induces conformational changes in the channel, which may thus become open or close.

According to Yellen (2002), the amazing combination of high selectivity and high permeability of potassium channels arises from several specific features of the channel architecture, as illustrated in Fig. 7.9 and described next.

- The permeation pathway contains water molecules, which help stabilize the ion in the pore – see label (1) in Fig. 7.9.
- The electrical dipoles inherent in every α-helix are oriented such that the negative end is oriented towards the center of the pore (2). This is assumed to introduce a preferential stabilization of the cations, thereby preventing the anions from entering the channel.
- As seen in chapter 1, positive ions dissolved in water are surrounded by the oxygen atoms of water molecules forming a hydration shell around the ion. The potassium channel contains a selectivity filter that mimics the structure of the hydration shell of the potassium ion in water (3), but not of other cations, such as Na^+. As seen in Fig. 7.9, the potassium ions in the channel form a chain in which individual ions are separated by a distance of about 7 Å (4), with hydration water interspersed along the chain.

In contrast to the potassium channels, chlorine channels are dimeric complexes, each monomer forming a barrel-like structure around its own pore (see Fig. 7.10).

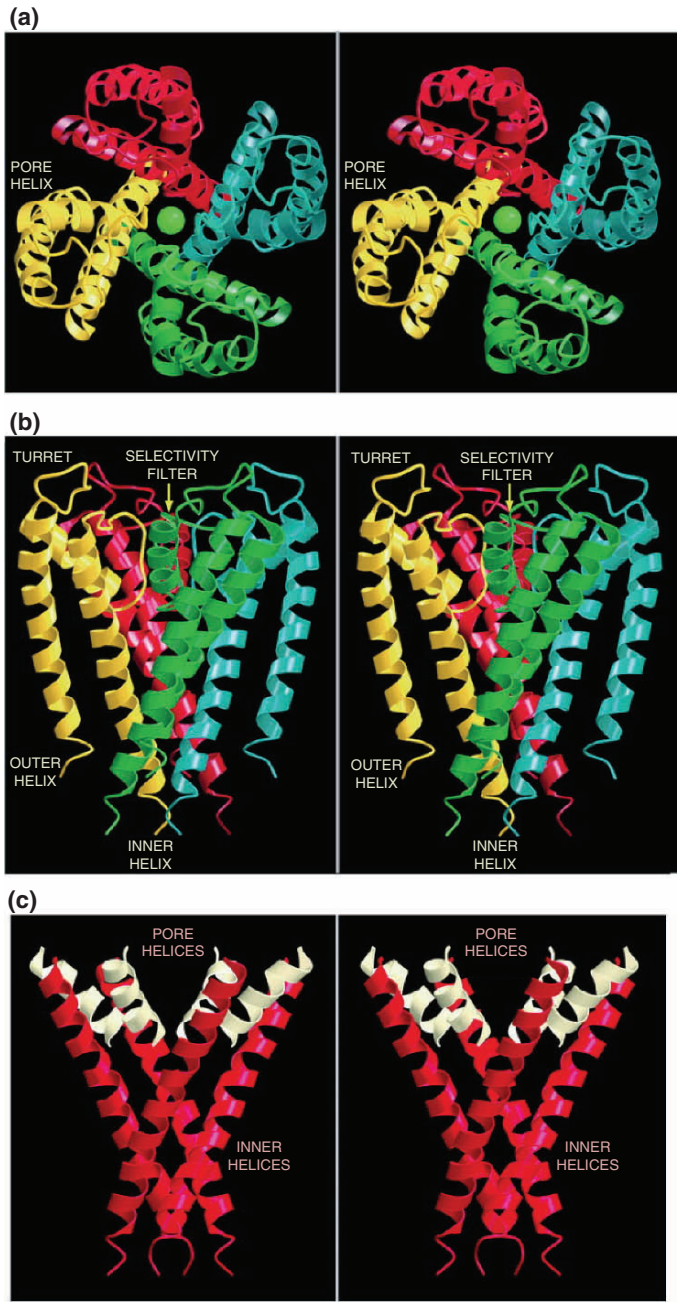

Fig. 7.8 Ribbon representation of a voltage-gated potassium channel (KcsA). (**a**) Stereo view illustrating the three-dimensional fold of the tetramer viewed from the extracellular side. Each color indicates a different subunit. (**b**) Stereo view from a direction contained in the membrane plane. (**c**) Stereo view of the inner helices only. Notice the top (white) helices creating a selectivity filter (Figure reproduced from Doyle et al., 1998).

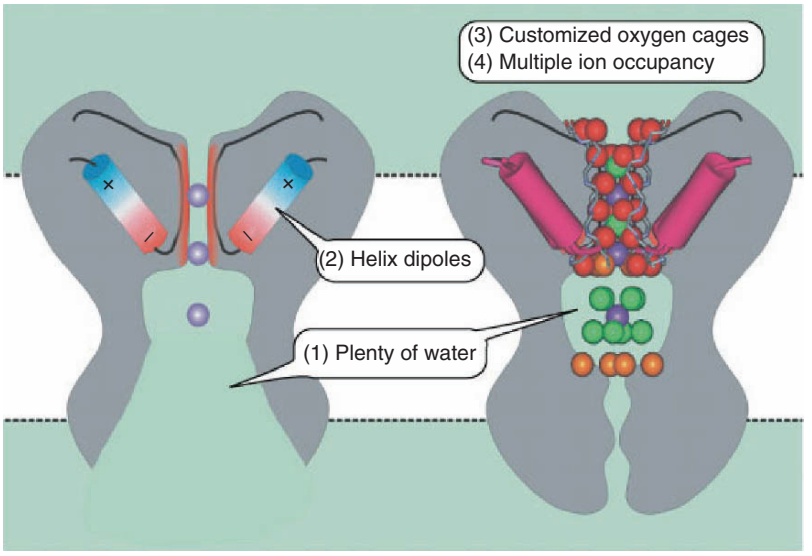

Fig. 7.9 Architectural features of K+channels leading to high selectivity and permeability. Potassium ions are represented by purple spheres, while the water appears in green (Cartoon from Yellen, 2002).

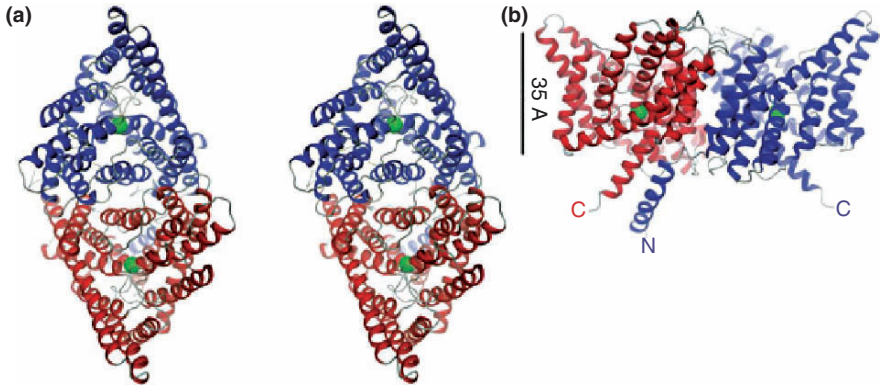

Fig. 7.10 (**a**) Stereo view of a ribbon representation of a chlorine-channel from the extracellular side. (**b**) View of the same channel from a direction within the membrane plane, with the extracellular side above the structure. The green spheres represent the selectivity filter of the Cl^- channel (Figure reproduced from Dutzler et al., 2002).

Other differences between Cl^- and K^+ channels include the absence of an aqueous cavity form the chlorine channels and, most notably, a negatively charged side chain of a glutamate amino acid. The latter is presumed to act as a gate that swings in and out of the diffusing pathway (Dutzler et al., 2002).

Potassium and chlorine channels, each actually constitutes large families of channels that are present in all plants and animal kingdoms. The slight differences

observed from channel to channel within a family of channels probably reflect the variety of specific roles ion channels play in different organisms as well as in different cell types of the same organism. On the other hand, the more notable differences between the two families of channels await further clarification.

Observation: In recognition of his important contributions to the structural and mechanistic characterization of ion channels, Roderick MacKinnon was awarded the Nobel Prize for Chemistry in 2003 (MacKinnon, 2003).

7.3 Ion Pumps

7.3.1 The Na-K-ATPase

On discussing the main ideas of active transport in chapter 4, we have postponed the discussion on the relation between the structure of the ion pump and its function. To be precise, there are several types of ion pumps, one of the most important being the *Na,K-ATPase*, already discussed in chapter 4. Na,K-ATPase is an integral membrane protein which couples the active transport of Na and K ions to ATP hydrolysis, and thereby acts as an enzyme for splitting the ATP into ADP.

The Na,K-ATPase is a *molecular machine* that pumps three Na ions out and two K ions into the cell per cycle, performed in about 10 ms (Alberts et al., 2002). Because, the concentration ratio of the transported ions is $[Na^+]/[K^+] = 3/2$, the pump has an *electrogenic* character (i.e., it contributes to the electrical polarization of the cell membrane) due to the net positive charge transferred outside the cell.

The global reaction describing the Na,K-ATPase function is:

$$3{Na^+}_{in} + 2{K^+}_{out} + ATP_{in} \rightarrow 3{Na^+}_{out} + 2{K^+}_{in} + ADP_{in} + P_{i,in} + \Delta G_{in} \qquad (7.7)$$

where, ADP is adenosine diphosphate, P_i inorganic phosphate, and ΔG_{in} is the Gibbs free energy involved in the reaction, which is of the order of $\sim -50\,\mathrm{kJ/mol}$ $(\sim -12\,\mathrm{kcal/mol})$.

Observation: Because at each cycle the ionic pump translocates simultaneously Na^+ out of the cell and K^+ into the cytosol, the pump is called an *antiport system* or, simply, an *antiporter*. If the two different ions are transported in the same direction, the transport system is called a *symport system* or *symporter*. If only one particle is transported in a single direction, the system is called a *uniporter* (e.g., carriers).

There are several variants of the Na,K-ATPase, all of which are composed of two types of protein subunits: α and β subunits (Kaplan, 2002; Hebert et al., 2003). The α-subunit is composed of ten transmebrane domains (helices) with a total molecular mass of approximately 110 kDa. A part of the α-subunit sticks out of the membrane into the cytoplasm and contains the *catalytic active site* of this pump, which is the site of ATP attachment and hydrolysis. The β-subunit has a single transmembrane domain with a molecular mass of 55 kDa. A short amino acid chain is exposed to the

cytosol, while a larger part of the subunit forms the glycosilated extracellular portion. The β-subunit plays an essential role in delivery and insertion of the α-subunit in the membrane. In addition to the α- and β-subunits, some Na,K-ATPase pumps have also a small γ-subunit with a molecular mass of about 7.3 kDa, which is believed to play a role in regulation of the enzymatic activity of the pump.

Apart from the crystal structure of some small fragments (posted on the Protein Data Bank, http://www.rcsb.org/pdb), a complete crystal structure of the Na, K-ATPase has not been obtained yet, due to the difficulty of obtaining 3D crystals. However, cryo-electron microscopy of two dimensional crystals in membranes (Herbert et al., 2003; Rice et al., 2001), together with other biophysical methods, furnished a rather complete picture of its structure. In addition, determination by Toyoshima et al. (2000) of the structure of a related ion pump, the Ca-ATPase, has allowed for useful comparisons to be made. Figure 7.11 shows outlines of the α- and β-subunits of the Na,K-ATPase.

In principle, the operation of the Na^+-K^+-ATPase is based on its ability to undergo *cyclic conformational changes* driven by the energy released from ATP hydrolysis. In the terminology used to describe enzymatic reactions, the series of successive conformational states of the pump are described by two main states: one with high

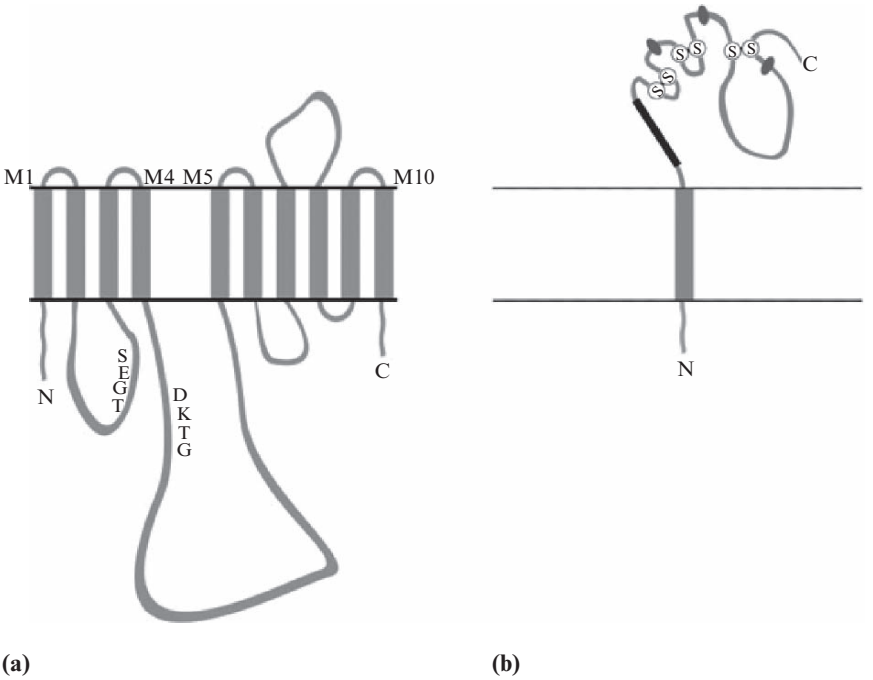

Fig. 7.11 Outline of (**a**) the α- and (**b**) β-subunit of the Na^+, K^+-ATPase. The heavy lines in the β-subunit indicate sequence involved in associations with the M7M8 loop of the α-subunit (Figures reproduced from Kaplan, 2002).

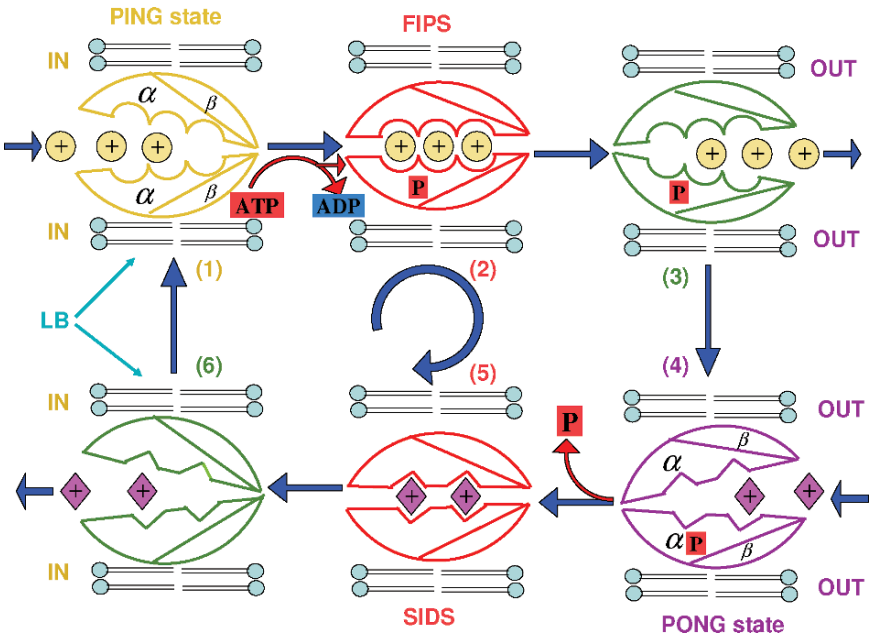

Fig. 7.12 The ping-pong mechanism accounting for the Na,K-ATPase functioning. Significance of the symbols: IN, OUT – extracellular, respectively intracellular space; FIPS – first intermediate phosphorylated state of the pump; SIDS – second intermediate dephosphorylated state. LB – lipid bilayers. Na ions are represented by circles and K ions by diamonds.

affinity for Na^+, which is called "*ping*," and another one with high affinity for K^+, called "*pong*." This "*ping-pong"* mechanism is illustrated in Fig. 7.12.

According to the ping-pong mechanism, the Na,K-ATPase is *phosphorilated* on its cytoplasmic side (α-monomer). This brings the pump into the *ping* state which is characterized by low affinity for K ions and very high affinity for Na ions. In this state, the pump binds three Na ions and undergoes a conformational change into a *first intermediate phosphorilated state* (FIPS), which leads to internalization of the Na ions. This is followed by the transition to the *pong state*, which is characterized by very low affinity for Na^+, the three captive Na ions being now released to the extracellular side of the membrane (where their concentration is already high). But, in the pong state, Na, K-ATPase presents a very high affinity for K^+ on the external side of the pump, which will now bind two K ions. This state is followed by the dephosphorylation of the α-subunit, which brings the pump into a *second intermediate dephosphorilated state* (SIDS), when the K ions are internalized within the membrane. In the "final" ping state, which presents low affinity for K^+, the two captive K ions are released inside the cell, where their concentration is already higher than outside. Thus, one full cycle of Na, K-ATPase active pumping of ions is complete, the pump being ready to enter the next cycle.

7.3.2 Other Ionic Pumps

In addition to the Na,K-ATPase, other ion pumps, such as H,K-ATPase, Ca-ATPase, K-ATPase, H-ATPase, and even light-activated proton pumps, may be found in the plasma membranes and organelle membranes of different types of cells (Stryer, 1988; Alberts et al., 2002).

H,K-ATPase, found in the cell membranes of the gastric mucosa (which plays a role in food digestion), maintains a very low pH of the gastric juice (Stryer, 1988), which is required for optimal functioning of different enzymes. The general equation describing the kinetics of reaction for this antiporter is:

$$nH^{+}{}_{in} + nK^{+}{}_{out} + ATP_{in} \rightarrow nH^{+}{}_{out} + nK^{+}{}_{in} + ADP_{in} + P_{i,in} + \Delta G_{in} \tag{7.8}$$

where n is an integer.

Ca-ATPase actively maintains a Ca^{2+} concentration difference of four orders of magnitude between the interior and the exterior of the cell (Alberts et al., 2002). The very low concentration of Ca ions in the cytosol $(0.1\,\mu M)$ is required for cellular signal transmission from an extracellular medium to the interior of the cell, by passive Ca^{2+} diffusion following specific chemical or physical triggers. The general equation describing the role of this *uniporter* is:

$$2Ca^{2+}{}_{in} + ATP_{in} \rightarrow 2Ca^{2+}{}_{out} + ADP_{in} + P_{i,in} + \Delta G_{in} \tag{7.9}$$

A particularly interesting ion pump is the H-ATPase, found in the membrane of some bacteria (e.g., *Halobacterium halobium* and *Escherichia coli*). This pump uses energy either from photons absorbed by a membrane pigment (the *bacteriorhodopsin*), in the case of *Halobacterium halobium* (Stryer, 1988), or from ATP hydrolysis, in the case of *Escherichia coli*, to transport H ions outside the cell against their concentration gradient. In their turn, proton concentration gradients across the membrane constitute a source of energy that may be used either to perform *chemical work* (i.e., to synthesize ATP in the dark in *Halobacterium halobium* cells), or to perform *mechanical work* (in the case of flagellated bacteria, such as *Escherichia coli* and *Salmonella thyphimurium*). In the latter case, the same ionic pump that expelled H^{+} outside the cell may operate in reverse (Berg et al., 2002).

Observation: In the case of *Halobacterium halobium*, when the H-ATPase is fuelled by ATP or light, it transports H^{+} outside the cell, creating an important proton concentration gradient. While in the dark, the bacterium expends the energy stored in this proton concentration gradient to synthesize ATP (chemical energy) needed for the cell metabolism. Therefore, the motor will operate in reverse, the H-ATPase, becoming an ATP-synthase. We are witnessing here an unexpected coupling between two processes with different *tensorial* orders: a *vectorial* process that transports molecules along a given direction (the passive diffusion) and a *scalar* process (the chemical reaction). This coupling could not take place in a homogeneous medium according to the *Curie Principle* (Prigogine, 1947), which in essence states that a scalar cause cannot produce a vectorial effect. However, the membrane and the cytosol are highly anisotropic structures, thereby favoring the coupling.

7.4 Light Absorption in Photosynthesis

In the previous chapters and also above in this chapter, we have discussed about conversion and use of energy in biological processes. But how did this energy come about in the first place? Organisms are thermodynamic systems that function far from equilibrium and which build and maintain their internal organization by consuming some sort of order from their environment, which Schrödinger called *negentropy* (Schrödinger, 1992). This is obtained from energy reservoirs in the universe – the stars (the Sun, in our case) – and is converted by *photosynthetic* organisms on the Earth (such as green plants and bacteria) and stored as free energy (Meszena and Westerhoff, 1999). The stored free energy is used in biological processes, for example to pump ions across the cell membrane against their concentration gradients, as discussed above. This section attempts to provide a thermodynamic description of the process of light absorption by special molecular machines involved in the processes of *photosynthesis* in green plants and bacteria.

7.4.1 Brief Overview of the Mechanism of Photosynthesis

Photosynthesis is a process of converting the light energy into bio-chemical energy, which consumes CO_2 and water and generates oxygen. As already mentioned in chapter 2, photosynthesis occurs in the *thylakoid* membranes of the specialized cell organelles – the *chloroplasts*. The main light-absorbing molecules in photosynthetic systems in bacteria and higher plants are *chlorophylls* and *carotenoids*. Chlorophyll molecules are bound into a protein complex, called the *light-harvesting system*, and arranged in space to form an *antenna* (Fig. 7.13) that efficiently absorbs light from the Sun and guide it to the two *reaction centers* where the conversion into free energy occurs (Gobets and van Grondelle, 2001; van Amerongen and van Grondelle, 2001; Atkins and de Paula, 2002; Berg et al., 2002).

The process of light-harvesting starts with absorption of photons by a chlorophyll molecule from the light-harvesting complexes, which is brought into an excited state, from where it decays within a few picoseconds (through nonradiative processes) to a state with lifetime of the order of nanoseconds (Nordlund and Knox, 1981). During its excited lifetime, there is a high probability that the chlorophyll looses its energy through resonance energy transfer to an unexcited nearby chlorophyll that has appropriate orientation relative to the first one (see chapter 8, for a brief description of the mechanism of resonance energy transfer, in a different context). The excitation can thus hop from chlorophyll to chlorophyll until it reaches a special chlorophyll called the *primary electron donor* of the reaction center, or chlorophyll P. The excited chlorophyll P transfers its energy to a chain of electron-transfer reactions that lead ultimately to storage of light energy into chemical energy, e.g., ATP and NADPH synthesis (Atkins and de Paula, 2002).

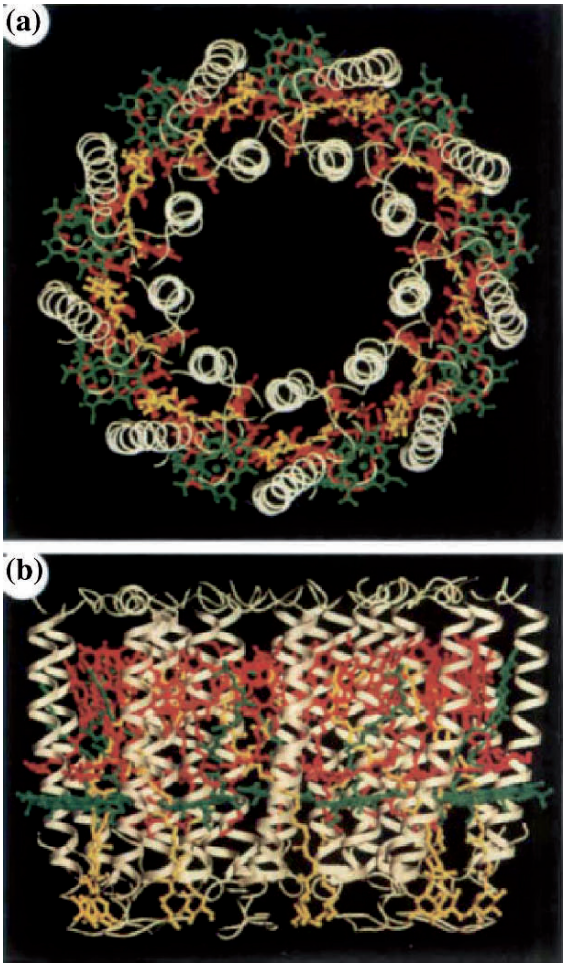

Fig. 7.13 Crystal structure of a light-harvesting complex from bacteria. (**a**) View of the complex from the cytoplasmic side of the membrane. (**b**) View from a direction perpendicular to the symmetry axis. Two types of chlorophyll a, B800 and B850, are shown in green and red color, respectively. The two chlorophylls absorb at 800 nm and 850 nm, respectively. The two chlorophylls are bound non-covalently to two hydrophobic apoproteins (shown in white) alongside with carotenoids (in yellow). The whole complex is an oligomer of these components (Figure reproduced from McDermot et al., 2002).

7.4.2 Thermodynamics of Light Absorption

In this section, we will introduce the thermodynamic aspects of the very first step in photosynthesis – the light energy absorption by chlorophyll. In doing so, we will follow closely the derivation presented by Lavergne and Joliot (2000).

Consider the "reaction" of *chlorophyll* excitation-deexcitation at equilibrium when monochromatic photons of frequency, ν, are absorbed and then are lost by chlorophyll:

$$Chl + h\nu \underset{k_d}{\overset{k_a}{\rightleftarrows}} Chl^* \tag{7.10}$$

where *Chl* stands for the chlorophyll in the ground state and Chl^* signifies the excited chlorophyll, k_a is the rate constant for light absorption and k_d is the rate constant for Chl^* de-excitation.

Since the process may be regarded as isotherm and isobar, populations of excited and unexcited chlorophylls may be described by chemical potentials, which we define here with respect to the number of molecules, N, as $\mu = \left(\frac{dG}{dN}\right)_{T,p}$. The two chemical potentials are:

$$\mu^{Chl} = \mu_0^{Chl} + k_B T \ln[Chl] \tag{7.11}$$

$$\mu^{Chl^*} = \mu_0^{Chl^*} + k_B T \ln[Chl^*] \tag{7.12}$$

where μ_0^{Chl} and $\mu_0^{Chl^*}$ are the standard chemical potentials of the two species and k_B is the Boltzmann constant, as usual.

If the system does not reach equilibrium, free energy may be extracted by converting Chl^* into *Chl*, which is proportional to the so-called *affinity*, defined by the difference of the chemical potentials described by equations (7.12) and (7.11), namely:

$$A = \mu_0^{Chl^*} - \mu_0^{Chl^*} + k_B T \ln \frac{[Chl^*]}{[Chl]} = \mu_0^{Chl^*} - \mu_0^{Chl^*} + k_B T \ln \frac{k_a}{k_d} \tag{7.13}$$

Note that the affinity is non-zero only if the system functions far from equilibrium, which should indeed be the case with the light-harvesting process in photosynthesis, where photon excitations are efficiently funneled towards a reaction center that converts energy in electrochemical form.

Assuming negligible changes in volume and entropy between the two states of the chlorophyll, then $dG = h\nu + pdV - TdS \cong h\nu$ (where h is Planck's constant), hence:

$$A = h\nu + k_B T \ln \frac{[Chl^*]}{[Chl]} = h\nu + k_B T \ln \frac{k_a}{k_d} \tag{7.14}$$

The concentration ratio in this equation may be determined from the Boltzmann formula:

$$\frac{[Chl^*]}{[Chl]} = \exp\left(-\frac{h\nu}{k_B T_{bb}}\right) \tag{7.15}$$

where the absorber is considered to be a black-body at a temperature, T_{bb} (Lavergne and Joliot, 2000; Meszena and Westerhoff, 1999). By combining the last two equations, we obtain immediately:

$$A = h\nu\left(1 - \frac{T}{T_{bb}}\right) \tag{7.16}$$

where the expression in the bracket is the yield of some Carnot machine that produces work from heat transfer between a "hot" source at temperature T_{bb} (a black body that absorbs energy from Sun) and a cold source (the external medium) at temperature T.

Quiz 2. Estimate the Carnot yield of the chlorophyll under light illumination with wavelength of 663 nm at the ambient temperature of 27 °C, assuming that the lifetime of the excited state is $1/k_a \cong 1\,\text{ns}$ (Nordlund and Knox, 1981) and that $k_d = 0.1\,\text{s}^{-1}$. Estimate also T_{bb}.

References

Alberts, B. A., Lewis, J., Raff, M., Roberts, K. and Walter, P. (2002) *Molecular Biology of the Cell*, 4th ed., Garland Science/Taylor & Francis, New York

Atkins, P. and de Paula, J. (2002) *Atkins' Physical Chemistry*, 7th ed., Oxford University Press, Oxford

Berg, J. M., Tymoczo, J. L. and Stryer, L. (2002) *Biochemistry*, 5th ed., W. H. Freeman, New York

Doyle, D. A., Morais Cabral, J., Pfuetzner, R. A., Kuo, A., Gulbis, J. M., Cohen, S. L., Chait, B. T. and MacKinnon, R. (1998) The structure of the potassium channel: molecular basis of K^+ conduction and selectivity, *Science*, **280** (5360): 69

Drenth, J. (1994) *Principles of X-Ray Crystallography*, Springer, New York

Dutzler, R., Campbell, E. B., Cadene, M., Chait, B. T. and MacKinnon, R. (2002) X-ray structure of a ClC chloride channel at 3.0 A reveals the molecular basis of anion selectivity, *Nature*, **415**: 287

Gobets, B. and van Grondelle, R. (2001) Energy transfer and trapping in photosystem I, *Biochim. Biophys. Acta*, **1507**: 80

Herbert, H., Purhonen, P., Thomsen, K., Vorum, H. and Maunsbach, A. B. (2003), Renal Na,K-ATPase structure from cryo-electron microscopy of two-dimensional crystals, *Ann. NY. Acad. Sci*., **986**: 9

Hille, B. (2001) *Ion Channels of Excitable Membranes*, 3rd ed., Sinauer, Sunderland, MA

Jentsch, T. J. (2002) Chloride channels are different, *Nature*, **415**: 276

Jiang, Y., Lee, A., Chen, J., Cadene, M., Chait, B. T. and MacKinnon, R. (2003) X-ray structure of a voltage-dependent K^+ channel, *Nature*, **423**: 33

Kaplan, J. H. (2002) Biochemistry of Na,K-ATPase, *Annu. Rev. Biochem*., **71**: 511

Kendrew, J. C., Bodo, G., Dintzis, H. M., Parrish, R. G., Wyckoff, H. and Phillips, D. C. (1958) A three-dimensional model of the myoglobin molecule obtained by X-ray analysis, *Nature*, **199**: 662

Lavergne, J. and Joliot, P. (2000) Thermodynamics of the excited states of photosynthesis, In: *BTOL-Bioenergetics*, chapter 2 (http://www.biophysics.org/btol/bioenerg.html)

MacKinnon, R. (2003) Potassium Channels and the Atomic Basis of Selective Ion Conduction, *Nobel Lecture*, http://nobelprize.org/nobel_prizes/

Malmivuo, J. and Plonsey, R. (1995) *Bioelectromagnetism*, Oxford University Press, New York

McDermott, G., Prince, S. M., Freer, A. A. Hawthornthwaite-Lawless, A. M., Papiz, M. Z., Cogdell, R. J. and Isaacs, N. W. (2002) Crystal structure of an integral membrane light-harvesting complex from photosynthetic bacteria, *Nature*, **374**: 517

Meszena, G. and Westerhoff, H. V. (1999) Non-equilibrium thermodynamics of light absorption, *J. Phys. A: Math. Gen*., **32**: 301

Neher, E. (1991) Ion channels for communication between and within cells, *Nobel Lecture*, http://nobelprize.org/nobel_prizes/

Neher, E. and Sakmann, B. (1976) Single-channel currents recorded from membrane of denervated frog muscle fibers, *Nature*, **260**: 799

Neher, E. and Sakmann, B. (1992) The patch clamp technique, *Sci. Am.*, **266**: 28
Nordlund, T. M. and Knox, W.H. (1981) Lifetime of fluorescence from light-harvesting chlorophyll a/b proteins. Excitation intensity dependence, *Biophys. J.*, **36**: 193
Prigogine, I. (1947) *Etude Thermodynamique des Phénomènes Irréversibles*, Desoer, Liége
Rice, W. J., Young, H. S., Martin, D. W., Sachs, J. R., and Stokes, D. L. (2001) Structure of Na^+, K^+-ATPase at 11 Å resolution: comparison with Ca^{2+}-ATPase in E_1 and E_2 states, *Biophys. J.*, **80**: 2187
Rhodes, G. (1993) *Crystallography Made Crystal Clear. A Guide for Users of Macromolecular Models*, Academic, San Diego, CA
Sakmann, B. (1991) Elementary steps in synaptic transmission revealed by currents through single ion channels, *Nobel Lecture*, http://nobelprize.org/nobel_prizes/
Sakmann, B. and Neher, E. (Eds.) (1995) *Single Channel Recording*, 2nd ed., Plenum, New York
Schrödinger, E. (1992) *What Is Life? The Physical Aspect of the Living Cell with Mind and Matter & Autobiographical Sketches*, Cambridge University Press, Cambridge
Stryer, L. (1988) *Biochemistry*, 3rd ed., W. H. Freeman, New York
Törnroth-Horsefield, S., Wang, Y., Hedfalk, K., Johanson, U., Karlsson, M., Tajkhorshid, E., Neutze, R. and Kjellbom, P. (2006) Structural mechanism of plant aquaporin gating, *Nature*, **439**: 689
Toyoshima, C., Nakasako, M., Nomura, H. and Ogawa, H. (2000) Crystal structure of the calcium pump of sarcoplasmic reticulum at 2.6 Å resolution, *Nature*, **405**: 647
van Amerongen, H. and van Grondelle, R. (2001) Understanding the energy transfer function of LHCII, the major light-harvesting complex of green plants, *J. Phys. Chem. B*, **106**: 604
Yellen, G. (2002) The voltage-gated potassium channels and their relatives, *Nature*, **419**: 35